Results in Physics 49 (2023) 106496

Contents lists available at ScienceDirect

Results in Physics

journal homepage: www.elsevier.com/locate/rinp

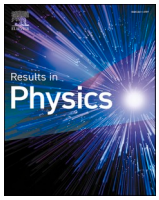

Fluid-Structure-Acoustic coupling analysis for external laminar and turbulent fluid flows

Tohid Adibi [a], Seyed Esmail Razavi [b], Shams Forruque Ahmed [c,*], Hussein Hassanpour [d], Neda Mohammadzadeh [b], S.M. Muyeen [e,*]

[a] School of Mechanical Engineering, University of Bonab, Bonab, Iran
[b] School of Mechanical Engineering, University of Tabriz, Tabriz, Iran
[c] Science and Math Program, Asian University for Women, Chattogram 4000, Bangladesh
[d] School of Automotive Engineering, Iran University of Science and Technology, Tehran, Iran
[e] Department of Electrical Engineering, Qatar University, Doha 2713, Qatar

ARTICLE INFO

Keywords:
Fluid-structure interaction
Acoustic coupling
Fluid flow
Elastic plate
Transmission loss

ABSTRACT

Controlling noise pollution is one of the most crucial parameters in various industries. The use of elastic plates has a substantial impact on noise pollution control and associated factors, such as transmission loss. Additionally, the transmission loss is affected by geometric variations. However, the effect of a rib and elastic plate on the acoustic properties of a channel for a wide range of Reynolds numbers has not yet been investigated, although their use could reduce noise pollution. This study thus investigates the acoustic and flow impacts of a rib and an elastic plate. The control variables for fluid-structure–acoustic coupling numerical simulations are rib height, rib angle, elastic plate length, elastic plate position, Reynolds number, and the Young module of the elastic plate. The governing equations are discretized using the Galerkin method. The results indicate that the transmission loss is 27% more at the elastic plate's highest position. By decreasing the length of the elastic plate by 50%, the mean transmission loss is reduced by 9%. The findings of this study can be utilized by mechanical and aerospace engineers in the design of aircraft, automobiles, and cooling and heating systems, particularly fan coils.

Introduction

To solve fluid flows or thermos fluid flows problems, solid boundaries are considered rigid. Nevertheless, in practical problems, solid boundaries are not rigid. The forces at the fluid-solid interface change the shape of the solid. Solid deformation affects the velocity and temperature fields. Hence, to obtain an accurate solution to these problems, it is necessary to solve the fluid flow governing equations and the solid body governing equations simultaneously. These problems are known as fluid-solid problems. Solid-fluid interaction is a destructive phenomenon in most engineering applications, and researchers have always searched for ways to study and control this phenomenon, such as flow-induced vibration (FIV) in mechanical systems. Different classifications can be introduced from different perspectives for this phenomenon. Vibrations induced by the output fluid in dams, the performance of fluid measurement systems, the phenomenon of induced vibrations in the aircraft wings, biological systems, marine systems, and the dynamic behavior of ships and vessels are some of these phenomena. Turbulent thermo-flow equations in conjunction with fluid-solid interaction (FSI) and acoustic transmission equations are applied to simulate the mentioned phenomena. In another view, noise is one of the leading causes of environmental pollution. Therefore, the noise generated by the devices must be controlled. Noise reduction can be shown as a loss in pressure inside the duct. The elastic plates and some structures like a muffler are applied for reducing the noise and disturbance created by the equipment.

FSI analysis has been performed in many studies. Chile and Zhang [1] reviewed the studies that ignored heat transfer, internal stresses, and plate thickness. Their work had been done experimentally. Accurate numerical methods were used in this work too. The results of numerical simulations were validated by that experimental work. Good agreement was seen and more simulations were done numerically. Turk and Hiron [2] considered solid boundary deformations in fluid flow. In their study, a flexible plate was attached to a rigid cylinder. They considered the flow two-dimensional and laminar and simulated it in three different inlet velocities. Hill et al. [3] simulated the flow through an elastic plate

* Corresponding authors.
E-mail addresses: shams.f.ahmed@gmail.com, shams.ahmed@auw.edu.bd (S.F. Ahmed), sm.muyeen@qu.edu.qa (S.M. Muyeen).

https://doi.org/10.1016/j.rinp.2023.106496
Received 27 November 2022; Received in revised form 11 April 2023; Accepted 25 April 2023
Available online 28 April 2023

attached to a rigid cylinder. They also plotted plate movement over time. Their results showed that the Monolithic solvers were more accurate than the segregated ones. Li and Yu [4] combined two numerical schemes to study the flow around an elastic plate attached to a cylinder. The cross-sections were circular and square. They investigated the drag coefficient for different Young modulus. In addition, the simulations were repeated for different cylinder diameters. They also stated that the vibration frequency of the oscillating plane is different from the plane's natural frequency. The results showed that the vibration frequency is different from the vortices' frequency too. In addition, they showed that the frequency of the oscillating plane does not depend on the sizes of the grids. Fu et al. [5,6] proposed a new analytical method to solve the Flexible plate problems. A numerical solution validated the accuracy of their method. The numerical simulation was performed by software employing a finite element scheme. Comparing the results of numerical and analytical methods revealed that the proposed analytical method is sufficiently accurate. In [7], Zhao and Fu contributed to the field of shape-memory materials. The simulations were conducted by ABAQUS software. Another study, namely an analytical study on microstructures was summarized by Fang et al. [8]. They reviewed the fabrication method in their work.

Tian et al. [9] numerically examined the flexible plate in two modes; in the first one, the density ratio of solid to fluid was ten, and in the second one, it was one. Nair et al. [10] numerically and experimentally investigated the flow around an elastic plate attached to a rigid cylinder. The Reynolds number of water flow in their study was equal to 30470. Their study shows that the Young modulus's size is very influential in plate oscillations. Khanafer et al. [11] simulated a flexible plate attached to a square-section cylinder in the channel with working fluid air. They also examined the effect of plate elasticity, inlet velocity, and cylinder size on the characteristics of thermos-fluid flow. They concluded that increasing the input speed causes harmonic oscillations in the plate. In addition, as the input speed increases, the vortices become more visible. Shi et al. [12] numerically investigated the increase in heat transfer by an oscillating plate in the airflow within a channel with elastic solid boundaries. The boundaries had a constant temperature. Two-dimensional flow is simulated numerically, and fluid in the inlet of the channel was considered at two different temperatures. The results show that heat transfer in this channel can increase up to 90%. The pressure drop is obtained too and the results demonstrate that increases in pressure drop are acceptable. Soti et al. [13] examined the effect of the elastic plate on Newtonian fluid and incompressible laminar flow within the channel. They simulated the flow in three cases; on the rigid cylinder, on the rigid plate attached to the rigid cylinder, and on the elastic plate attached to the rigid cylinder. They also investigated the effect of Reynolds number, Prandtl number, and material properties on fluid flow parameters. The results show that the mean Nusselt number increases up to twice by using an elastic plate connected to the rigid cylinder. Yoshinaga et al. [14] performed a one-dimensional aeroacoustics flow numerical simulation. The result shows that the fast variation in the flow rate formed a vigorous source. Xiaoji et al. [15] proposed a novel scheme to simulate turbulent flow restricted in elastic borders. Springer et al. [16] studied the aero-acoustics and the vibrio-acoustic sound radiations numerically. The turbulent flow inside an elastic solid channel is simulated. Prajapati et al. [17] studied the fluid-structure acoustic thermo-flows numerically. The flow was turbulent and direct numerical simulation was used to analyze it.

Pitchaimani et al. [18] performed a simulation for a two-dimensional flow inside a cavity with elastic solid boundaries. The influence of different geometry and different physical properties on the flow characteristics was elaborated. The results were compared with the outcomes of the rigid boundaries. Significant differences were observed. Torregrosa et al. [19] performed experimental and numerical analysis on a fluid-structure-acoustic coupling problem. The results show that numerical outputs validated by the experimental one are very good. Considering the results of this paper and the fact that numerical methods are much less expensive compared to experimental methods, it can be expected that more researchers will use numerical methods to analyze complex fluid-structure-acoustic coupling problems. Lam et al. [20] used the direct aeroacoustics simulation of a fluid-structure coupling problem. The flow inside an elastic cavity with different boundary conditions was simulated in this work. The simulations were performed in low Mach numbers. Massimo et al. [21] performed an experimental analysis using Laser Doppler Velocimetry for a three-dimensional fluid-acoustic coupling problem. The flow was laminar and incompressible. Borvornsareepirom and Rojanaratanangkule [22] simulated a two-dimensional external flow over a plate at a high Mach number. Compressible flow governing equations were solved according to the Mach number. The Reynolds number was 1000 and the flow was laminar. The influence of Mach and Reynolds numbers on the acoustic noise was surveyed. Purohit et al. [23] simulated a two-dimensional acoustic flow over a flexible plate numerically. The influence of geometry on the fluid-structure-acoustic characteristics was surveyed. Simulations were done for different velocities of fluid and the hardness of solid. They detected that the significance frequency is marginally different from the natural vibration frequency of the flexible boundaries.

As evidenced by the relevant literature, the effect of a rib and an elastic plate on the acoustic characteristics of laminar and turbulent flows has not yet been investigated. The present work is the first to simulate the fluid-structure-acoustic interaction in a channel featuring a rigid rib and an attached elastic plate. At laminar and turbulent regimes, the influence of varied rib and elastic plate geometries is studied numerically. In addition, the effects of various materials are examined. These findings could be utilized by mechanical and aerospace engineers in the design of aircraft, automobiles, and cooling and heating systems, particularly fan coils. This research could reduce noise levels in air conditioning systems and other factories. As a result, it will benefit workers in a range of industries and reduce noise pollution in the workplace.

Mathematical modeling

The fluid-solid interaction simulation is one of the most complex problems in computational fluid dynamics. In these problems, the governing equations for fluid flow and the flexible solid body should be solved at the same time. In this section, the governing equations are presented. The continuity equations or conservation of mass in a fluid flow is generally expressed as equation (1) [24].

$$\nabla.\boldsymbol{v} = 0 \tag{1}$$

In equation(1), v is the velocity vector. The momentum equations for viscous and incompressible Newtonian fluids are expressed as equation (2) [24].

$$\rho\frac{\partial V}{\partial t} = \nabla\tau_u \tag{2}$$

In equation (2),v is the velocity vector andτ_u is the stress tensor. Discretization of the equation becomes three equations in three directions of coordinates. The stress tensor is expressed as follows:

$$\boldsymbol{\tau_u} = -p\boldsymbol{I} + \boldsymbol{\tau}, \boldsymbol{\tau} = \mu\left[\nabla.\boldsymbol{v} + (\nabla.\boldsymbol{v})^T\right] \tag{3}$$

Where μ is the viscosity of a fluid, p is the pressure, and I is the identity tensor. Three sets of equations are required for a flexible solid body. The first is the stress equilibrium equation [25]:

$$\bar{v}.\sigma + f = pa \tag{4}$$

Where f is volumetric forces, a is the acceleration, and σ is the Cauchy stress tensor. There are nine unknowns in these three equations. The following equations are strain–displacement relations that represent the deformations of the body in proportion to the displacement [25]:

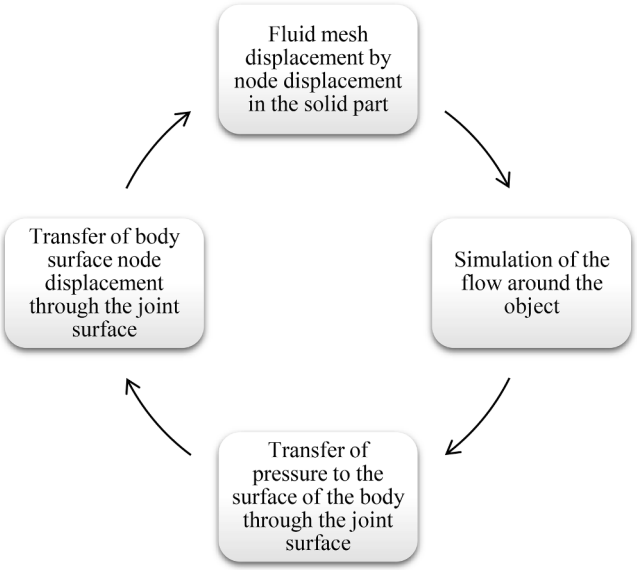

Fig. 1. Stepwise simulation Process.

$$\varepsilon_{ij} = \frac{1}{2}\left(\frac{\partial u_i}{\partial x_j} + \frac{\partial u_j}{\partial x_i} + \frac{\partial u_k}{\partial x_i}\frac{\partial u_k}{\partial x_j}\right) \tag{5}$$

Where ε is the strain, and u_i is the displacement in the x-direction. For minor strains, partial derivative terms can be ignored. Another six equations are required to solve the system of equations that relate the mechanical properties of the model to stress and strain. The material used in this paper is linear and isotropic elastic, so Equation (6) is as follows [25]:

$$\sigma_{ij} = \frac{E}{1+v}\left(\varepsilon_{ij} + \delta_{ij}\frac{v}{1-2v}\varepsilon_{kk}\right) \tag{6}$$

Where E is Young's modulus, v is Poisson's coefficient and δ is the Kronecker delta. The governing equations are solved numerically. Due to the deformation and displacement of the joint fluid-solid boundary, the grid deformation equations must also be solved. Fig. 1 shows the flow simulation steps. The simulation continues until the convergence criterion is reached.

The discretization of displacement and diffusion terms is performed with a second-order accuracy scheme, and the turbulence model used in this research is the standard $k-\varepsilon$ model. This method shows the transfer of spectral energy better. Another advantage of this model is that the dissipation term has no singular point, even if k reaches zero or becomes negative. This model has been measured for various flows such as jet streams, interference layers, intra-channel flows, boundary layers, homogeneous rotational shear flows, and separating flows. The standard $k-\varepsilon$ turbulence model is a quasi-experimental model-based. The

Table 1
Different parameters for simulations.

Model	1	2	3	4	5	6	7	8
Variable	a/h	e/h	b/h	c/h	f/h	α	E (MPa)	Re
Variations	5	0.2	0.8, 1.2, 1.6	15	0.25, 0.5	−45, 0, 45	0.1, 1, 10	100, 4000

modeled transfer equation k is obtained from an explicit equation, while the modeled transfer equation ε can only be justified by physical reasoning and is therefore very similar to the explicit equation k. In the development of the standard $k-\varepsilon$ model, it is assumed that the flow is entirely turbulent, and the effects of molecular viscosity are ignored. The transfer equation of the turbulent kinetic energy model k and the depreciation rate ε are two equations [26].

$$\frac{\partial(\rho K)}{\partial t} + \frac{\partial(\rho K u_i)}{\partial x_i} = \frac{\partial}{\partial x_j}\left\{\left(\mu + \frac{\mu_t}{\sigma_K}\right)\frac{\partial K}{\partial x_j} + G_K + G_b - \rho\varepsilon - Y_b\right. \tag{7}$$

$$\frac{\partial(\rho\varepsilon)}{\partial t} + \frac{\partial(\rho\varepsilon u_i)}{\partial x_i} = \frac{\partial}{\partial x_j}\left\{\left(\mu + \frac{\mu_t}{\sigma_\varepsilon}\right)\frac{\partial \varepsilon}{\partial x_j} + C_{\varepsilon 1}\frac{\varepsilon}{K}(G_K + C_{\varepsilon 3}G_b) - C_{\varepsilon 2}\rho\frac{\varepsilon^2}{K}\right. \tag{8}$$

In Equations (7) and (8), G_K is the kinetic energy of the turbulence K under the influence of the mean velocity gradient, and G_b is the kinetic energy of the turbulence K under the buoyancy force. Y_b is the oscillating expansion in the turbulence of the depreciation rate. $C_{\varepsilon 1}.C_{\varepsilon 2}.C_{\varepsilon 3}$ are experimental constants. σ_K and σ_ε are also chaotic Prandtl numbers. The experimental constants and Prandtl numbers are as follows [26]:

$$C_{\varepsilon 1} = 1 \bullet 44\ C_{\varepsilon 2} = 1 \bullet 92 C_{\varepsilon 3} = 0 \bullet 09 \sigma_K = 1 \sigma_\varepsilon = 1 \bullet 3 \tag{9}$$

Where $k = 2\pi f/c_0$ is the wavelength and c_0 is the speed of sound. q is the polarity term, which is equal to the acceleration per unit volume and is assumed to be zero in this paper. With this expression, the solution in the frequency range can be done parametrically. The transmission loss in the channel can be calculated as follows [27]:

$$TL = 10\log(p_{in}/p_{out}) \tag{10}$$

Where p_{in} and p_{out} represent the power of incident wave coming towards the control volume and the power of transmitted wave going away from the control volume.

The transmission loss is the channel's acoustic pressure input and output. This loss is independent of the noise source and depends on the channel structure. Noise generated by the system as a source of noise pollution must be controlled. The governing equations, including continuity equations, momentum equations, and Helmholtz equations, were presented in the acoustic analysis along with the boundary conditions of the problem. The integral function of the transmission loss at the input and output is used in the acoustic analysis of the flow inside the channel. The elastic plate exhibits muffler-like behavior and can therefore help reduce the noise created by the equipment. Noise reduction can be

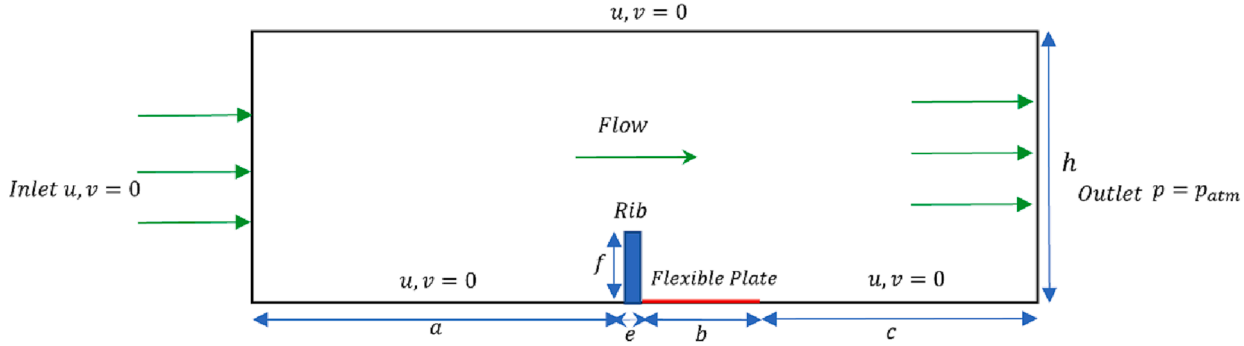

Fig. 2. Schematic of the channel, elastic plate, and rib.

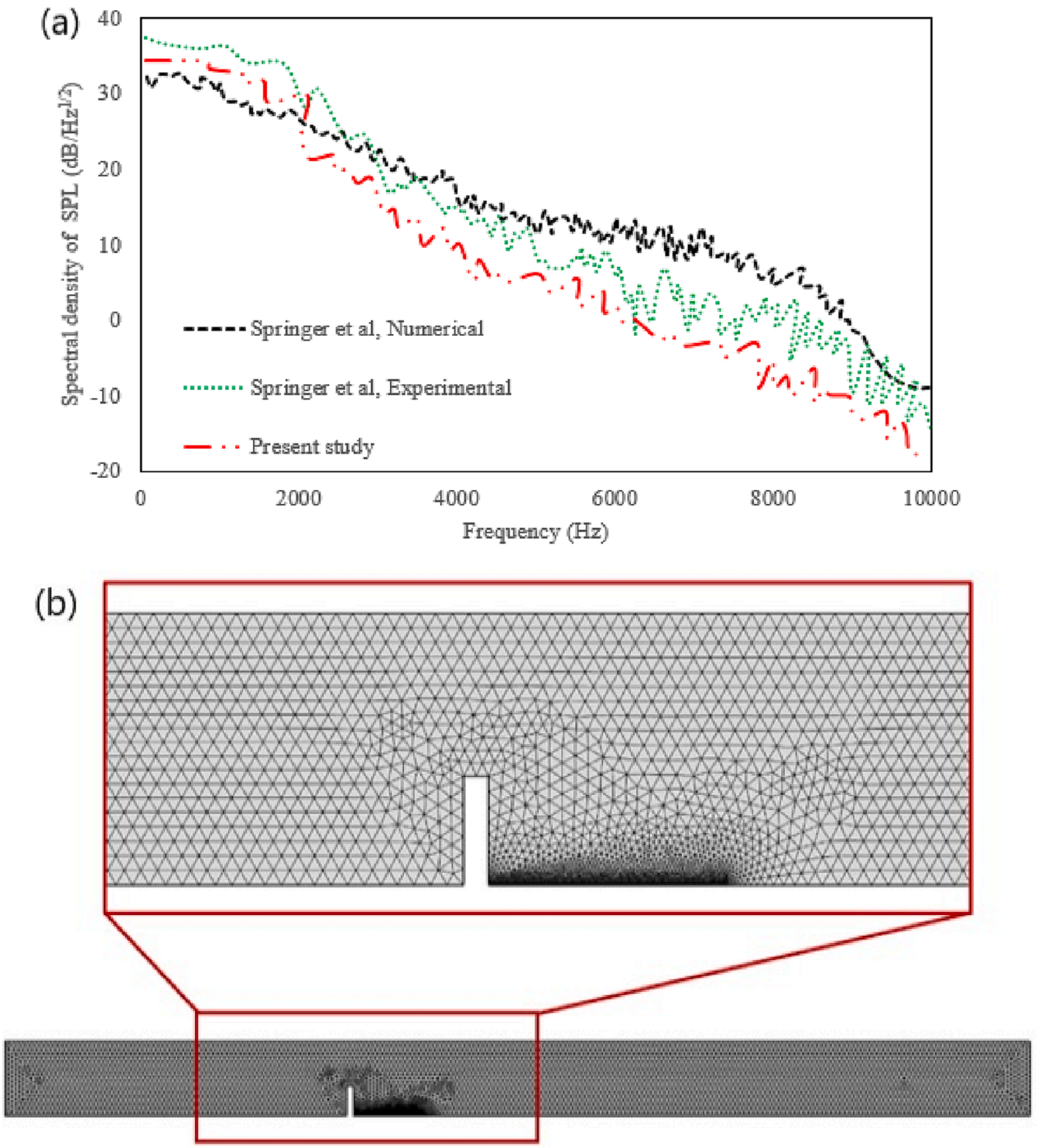

Fig. 3. A) Distribution of sound pressure density spectrum against frequency (validation is done with the works of springer et al. [28]) b) Channel with elastic plate and rib with zoom-in grid.

shown as a drop in pressure inside the duct. The geometry of the channel, along with the elastic plate and the rib, is shown in Fig. 2. Simulations are done for different parameters which are shown in Table 1.

In the Table 1, a is the distance between the inlet and rib, b is the elastic plate length, c is the distance between the elastic plate and outlet, h is the outlet height, e is the rib thickness, and f is the rib height. Alpha (α) is the angle between the rib and the elastic plate. E is the elasticity modulus, and the *Re* is the Reynolds number. The velocity in the x and y direction is given in the inlet and the pressure in the outlet is known too. These are hydraulics boundary conditions. In addition, no-slip condition is considered in the walls. Changing each of the variables in Table 1 leads to different results that make it possible to discuss changes in flow characteristics such as pressure, stress, velocity, and noise.

Results and discussion

Various numerical simulations are done and the results are reported

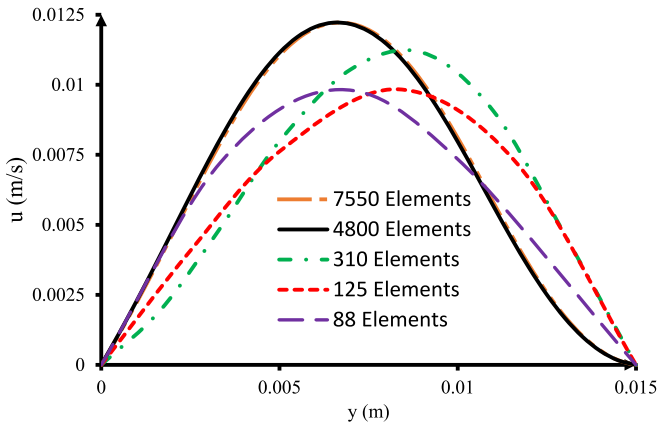

Fig. 4. Comparison of horizontal velocity at the channel output for different grid sizes.

and discussed in this part. Validation and grid independence should be done in the first step. Hence, to verify the results of the present simulation are compared with the results of Springer et al. [28]. They simulated the turbulent flow inside a channel with a rib and an elastic plate. The experimental and numerical simulations were done by Springer et al [28]. The validation is done with numerical and experimental results in Fig. 3a. The used grid is shown in Fig. 3b. An unstructured triangle grid is used.

The computational time and stability are disrupted by increasing the number of elements. Therefore, making selected grids finer does not always increase the accuracy of the solution. The grid independence is done to find and use the optimum grid. The grid independence is done in this work and is shown in Fig. 4. As it is observed, changing the grid, the horizontal velocity components inside the channel change, but this change is minimal between grid numbers 4 and 5. In other words, the results in the grid with 4800 cells have a negligible difference from the results in the grid with 7550. Therefore, grid number 4 is chosen for numerical simulations.

In this paper, the effect of the existence of an elastic plate after the rib on the flow behavior inside the channel is investigated. The results are displayed as velocity and pressure contours, and in addition, pressure, velocity, and displacement diagrams are plotted in different figures. First, the influence of the elastic plate's location after the rib inside the channel for different Reynolds numbers is surveyed. Fig. 5 shows the velocity and pressure contours for different positions of the elastic plate at Re = 4000. As shown in Fig. 5, areas of high pressure are located upstream before the rib, whereas areas of low pressure are located downstream after the rib and elastic plate. Behind the rib, vortices form due to the boundary conditions. Moreover, by examining the velocity profiles, it is evident that the velocity has increased as the area at the location of the rib has decreased. According to the law of conservation of mass for incompressible flows, a decrease in cross-section results in a rise in average velocity. In addition, the velocity decreases when approaching stationary walls and reaches zero on the walls due to the non-slip condition law. The results of Fig. 5 therefore appear to be accurate. At Reynolds numbers of 100 and 4000, simulations have been performed. At *Re* = 100, the flow is considered as laminar. As the Reynolds number increases above 2000 in the channel's flows, disturbances within the flow form and develop. High Reynolds numbers result in turbulent flow because the presence of ribs and elastic plates generates more flow disturbances.

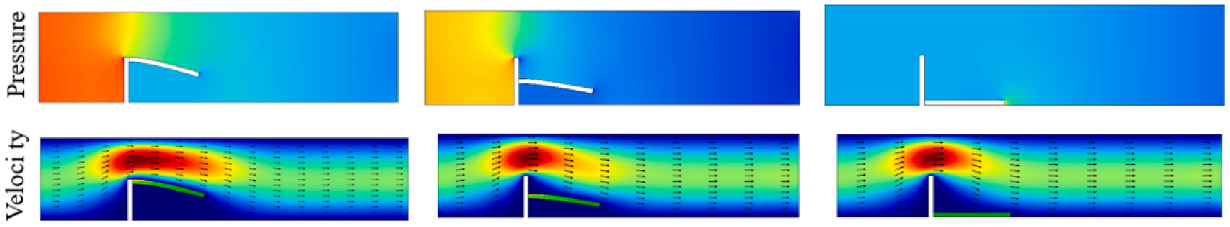

Fig. 5. Velocity, and pressure contours for different positions of the elastic plate at Re = 4000.

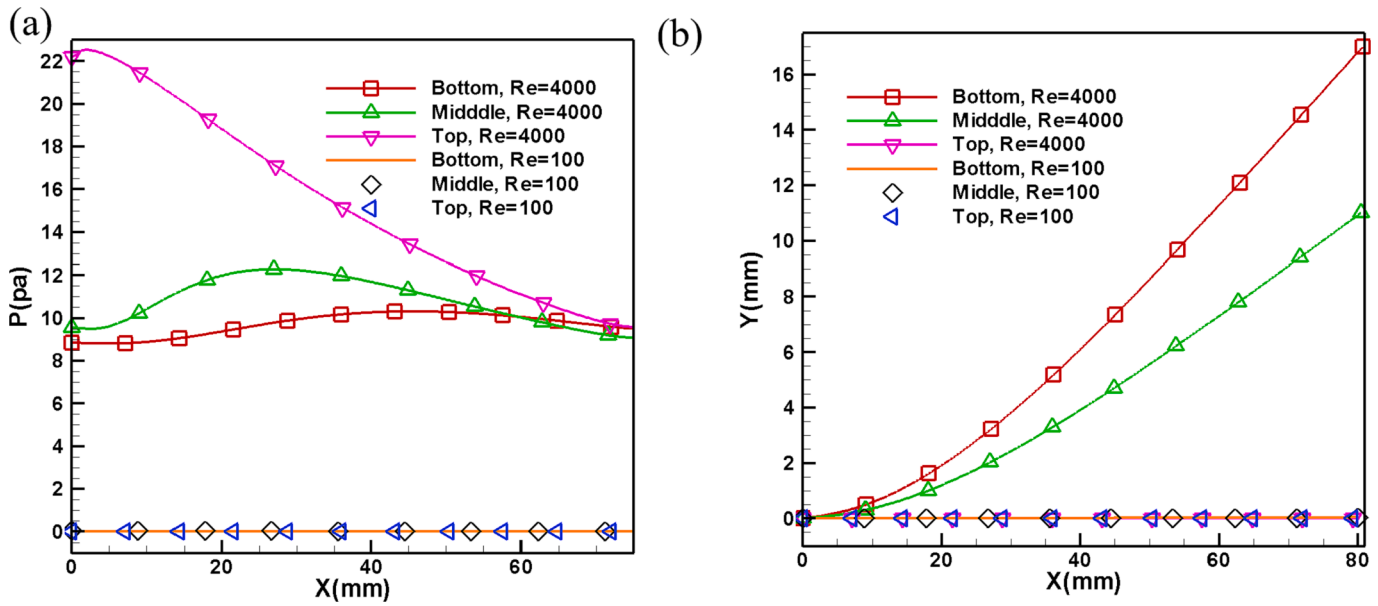

Fig. 6. A) Pressure variation on the elastic plate at different reynolds numbers b) displacement of the elastic plate in different positions and reynolds number.

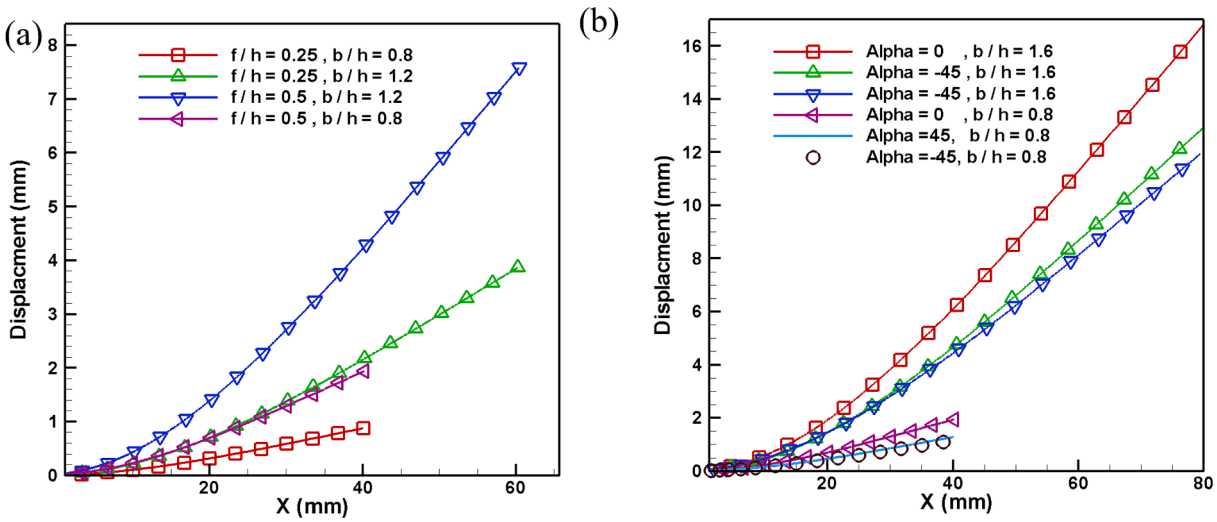

Fig. 7. A) Displacement of the elastic plate changes with changing plate length and rib height b) displacement variation of the elastic plate by changing the rib angle and the length of the elastic plate.

As seen in Fig. 5, the velocity contour shows the most significant change on the elastic plate at the top position attached to the rib. The pressure field is affected by the impact on the rib, and the most negligible change is for the elastic plate attached to the channel floor. The rib cause different vortices in the channel. The combination of rib and elastic plate changes the position and power of the vortices. The least effect on vortices happens when the elastic plate is in the bottom position and the most effect on vortices happens when the elastic plate is at the top position. When the elastic plate locates at the top position, the pressure of space between the elastic plate and rib reduces and a weak vortex is formed in this space. The flow pattern changes a lot in this position, especially in high Reynolds numbers. Pressure distribution on the elastic plate shows more detail of flow characteristics. Hence, the pressure is obtained on the elastic plate in different Reynolds numbers and different positions of the elastic plate and is shown in Fig. 6a.

As observed in Fig. 6a, pressure variation at low Reynolds numbers is less than its variation at high Reynolds numbers. The velocity of the fluid and its variation in the flow field is greater at high Reynolds numbers. As a result, the pressure variation is higher too. The vortex is made by the rib and covers the region above the elastic plate. Consequently, the pressure and its variation are low when the elastic plate is in the bottom position. However, when the elastic plate locates in a high position, the elastic plate separates the high and low-pressure regions. Hence, the pressure and its variation on the top part of the elastic plate are higher in this position. The pressure variation chart has a maximum valve. The maximum pressure happens near the first point of the elastic plate when the elastic plate locates at a high position. This maximum pressure occurs near the end of the elastic plate when the elastic plate locates at the bottom part of the channel. When the elastic plate locates at the top position, the low and high-pressure regions reach together at the end of the elastic plate and as a result, the minimum pressure is on the end of the elastic plate. When the elastic plate locates at the bottom part, the vortex on it cause a low-pressure region, and the pressure on the plate is low. The combination effect of rib and elastic plate makes a complex flow and hence, the maximum pressure happens at different points according to the different boundary conditions. The displacement of the elastic plate in different positions and different Reynolds numbers is shown in Fig. 6b.

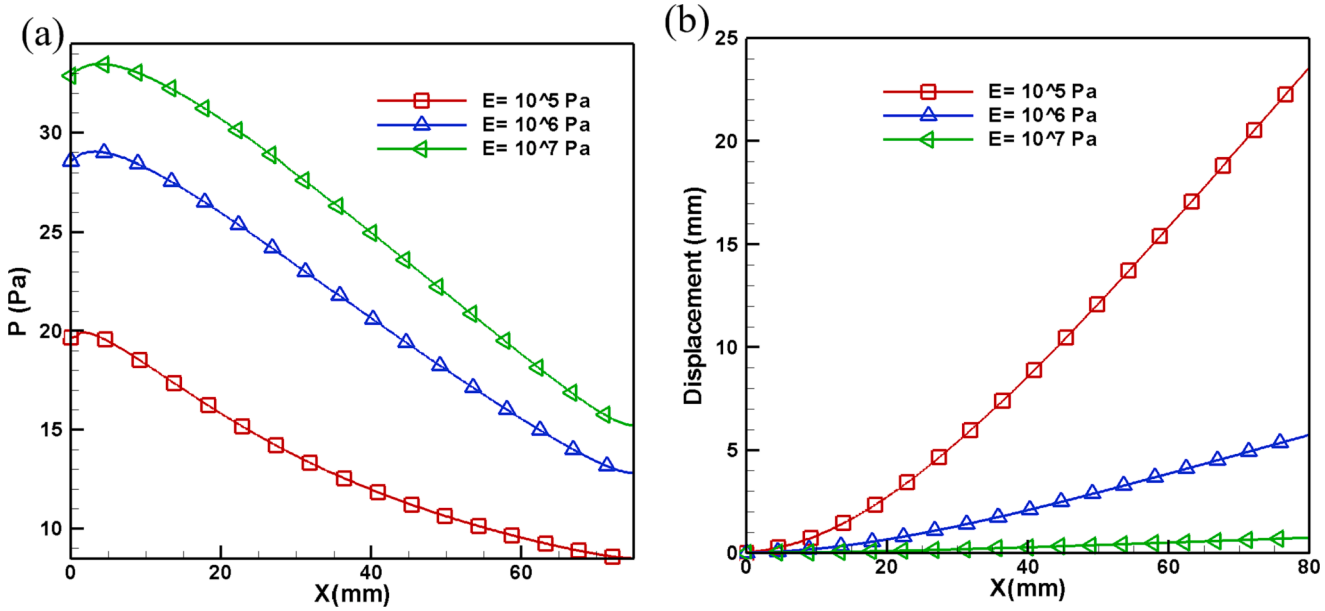

Fig. 8. A) Variation of the pressure on the elastic plate at different young's modulus b) displacement of the elastic plate with different materials.

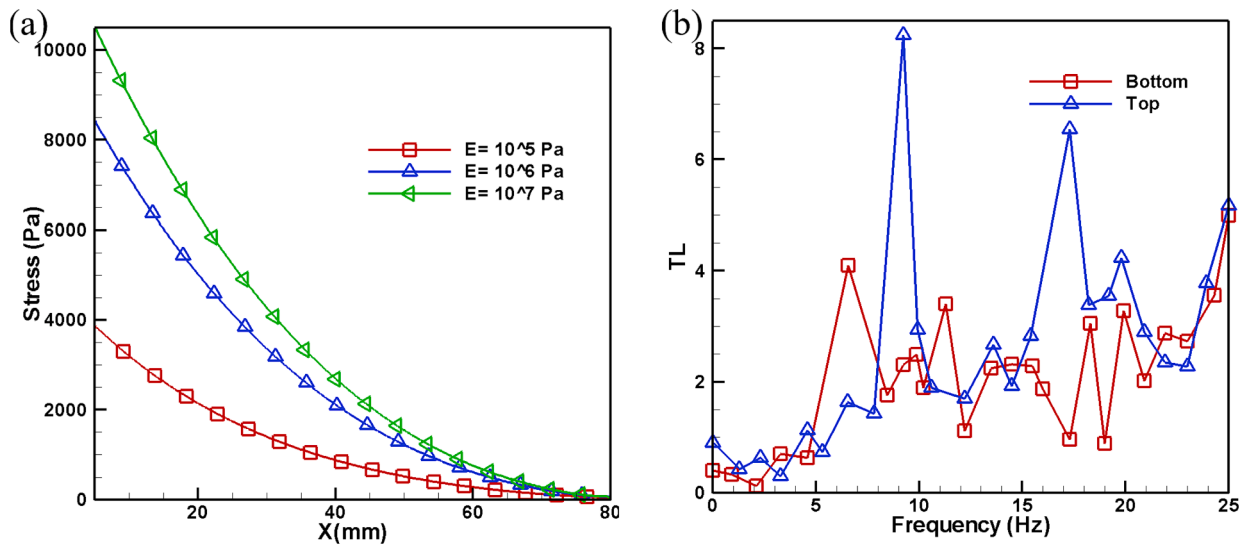

Fig. 9. A) The von mises stress on the elastic plate due to flow in different types of plates b) transmission loss versus frequency at different positions of the elastic plate.

Fig. 6b shows that the displacement of the elastic plate at the top position attached to the rib at high Reynolds is greater than its value at other positions and low Reynolds. When the elastic plate is at its highest, the pressure distribution on its two sides is the most different. The reason is the presence of vortices under the elastic plate. The existence of vortices under the elastic plate creates a wide low-pressure region. The large difference between the upper and lower pressure of the elastic plate causes the forces to be downward. Because of this force, the elastic plate bends downward and the internal forces of the plate create a new statics state. Deformation of the elastic plate causes a slight change in the flow characteristics. All the mentioned cases become weaker as the elastic plate goes down, and the least changes are when the elastic plate is in its lowest state. As the Reynolds number decreases, the velocity in the channel decreases. Decreasing the velocity reduces the velocity and pressure gradients and reduces the strength of the vortices. Therefore, by reducing the Reynolds number, the displacement of the elastic plate decreases.

Fig. 7a illustrates the displacement Variation for the different lengths and heights of the rib and the plate. Fig. 7a shows that the maximum plate displacement occurs at high rib heights and plate lengths. As the length of the separator increases, the elastic plate is placed at a higher height. As a result, the pressure difference between the top and bottom of the elastic plate increases, and the vertical displacement of the elastic plate increases. The points closer to the support have less displacement. In addition, with the increase in the length of the elastic plate, the vertical displacement of the endpoint in the plate increases. When the elastic plate bends, the velocity and pressure fields change a little. The displacement variation for different angles and lengths is shown in Fig. 7b. The reduction in length at any angle of the rib leads to a decrease in the displacement of the elastic plate. The maximum displacement is shown in the vertical position of the rib.

Pressure changes due to flow on the elastic plate by changing the material of the plate with the maximum length are shown in Fig. 8a. The pressure on the plate increases with increasing Young's modulus. The

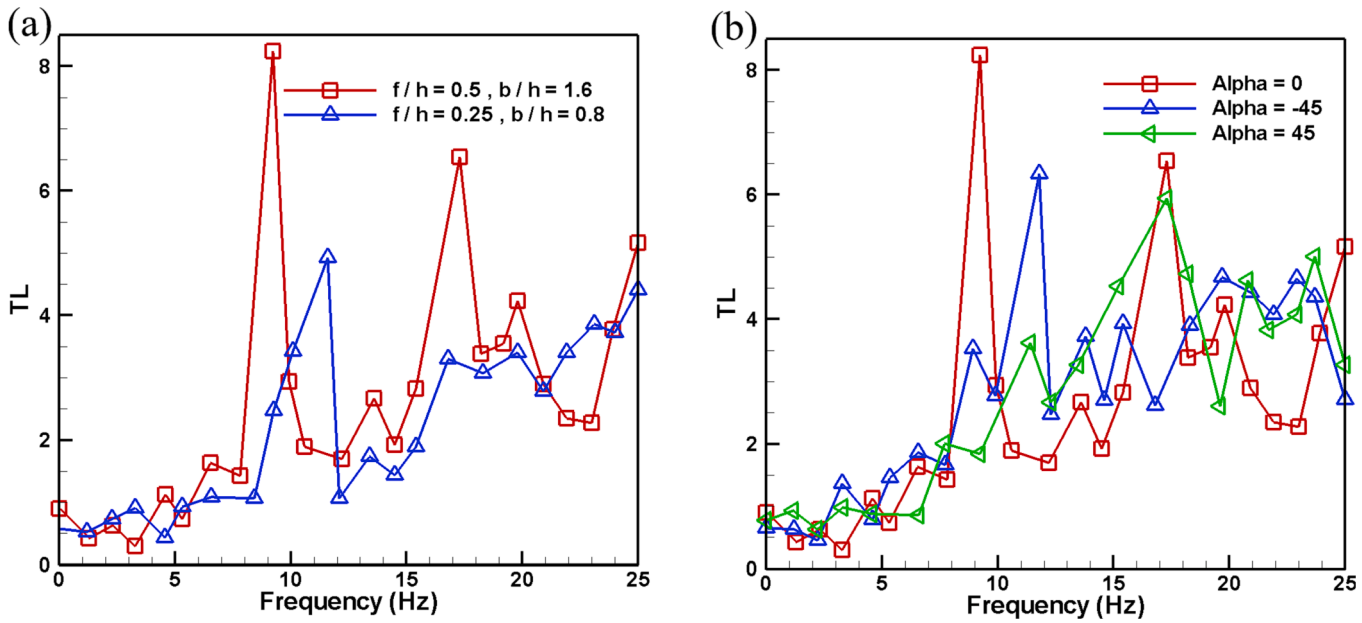

Fig. 10. a) Transmission loss versus frequency at different geometry of the elastic plate b) Transmission loss versus frequency at different rib angles.

material with a high Young's modulus is more hardened than the materials with a low high Young's modulus. As a result, the material with high Young's modulus resistance is more to deform. Consequently, the elastic plate supports higher forces. In other words, the pressure gradient becomes more in the elastic plate with a higher Young's modulus. Fig. 8b shows the displacement of the elastic plate at different Young's modulus. With the increase of Young's modulus, the material that makes up the elastic plate becomes harder. As a result, it is more resistant to deformation. At a higher Young's modulus, the elastic plate behaves like a rigid plate, and therefore, its deformation becomes very small.

Fig. 9a shows the Von Mises stress on the elastic plate by changing its characteristics. As the hardness of the elastic plate increases, the stress inside it increases. The stress in the support has the highest value, and in a downward trend, its value reaches zero at the free end of the elastic plane. The change for stress along the length of the beam has a decreasing trend, and the highest stress gradient is observed in the support. Transmission loss can detect the amount of noise coming out of the equipment. It determines the level of acoustic pressure in the input and output of a device. The pressure drop and transmission loss depend on the geometric structure of the device. The operating frequency range of the device is also effective in the pressure drop and transmission loss. Fig. 9b demonstrates the influence of the position of the elastic plate on transmission loss. Transmission loss depends on frequency highly.

Mean transmission loss for a higher position of the elastic plate is more as is observed in Fig. 9b. The mean transmission loss for the higher position of the elastic plate is 2.65 and for the lower position of the elastic plate is 2.09. Therefore, the transmission loss is 27% more in the highest position of the elastic plate. The influence of the length of the rib and elastic plate on transmission loss is shown in Fig. 10a for different frequencies. Fig. 10 shows that shortening the elastic plate not only changes the peak location of the graph but also reduces its number Mean transmission loss for a long elastic plate is more than the short one. The mean transmission loss for a long elastic plate is 2.65 and for a short length of the elastic plate is 2.22. Then By reducing the length of the elastic plate by 50%, the mean transmission loss decreases by 9%. The effect of the angle of the elastic plate on transmission loss is shown in Fig. 10b for different frequencies. The mean transmission loss for $\alpha = -45$ is 2.86, for $\alpha = 45$ is 2.85, and $\alpha = 0$ is 2.65.

Conclusion

Using the fluid-structure-acoustic coupling method, a numerical analysis of a fluid inside a channel with an elastic plate attached to the rib has been performed in this paper. Fluid flow and characteristics including pressure, velocity, and frequency have been investigated for the existence of rib and elastic plates. The influence of different parameters such as plate length, plate position, rib angle, rib height, plate material, and Reynolds number on flow characteristics have been studied. The Galerkin method has been applied in a finite element simulation framework. The mean transmission loss for the elastic plate's higher position was found to be 2.65, while the mean transmission loss for the lower position was determined to be 2.09. These results indicate that the transmission loss is 27% more at the elastic plate's highest position. By reducing the length of the elastic plate by 50%, the mean transmission loss is decreased by 9%. Additionally, the mean transmission loss is 2.86 for $\alpha = -45$, 2.85 for $\alpha = 45$, and 2.65 for $\alpha = 0$. The highest displacement of the elastic plate occurs when it is attached to the top of the rib, and its displacement decreases when the position is changed and the Reynolds number is decreased. Flow damping occurs at higher induced frequencies when Young's modulus of the plate is lower and the plates appear more rigid. As the plate advances along its length, the displacement and slope increase. Increasing the slope increases the displacement faster. As the modulus of elasticity increases, the displacement of the plate decreases and there is an almost linear relationship between displacement and elasticity modulus. So that when the elasticity modulus increases tenfold, it decreases almost tenfold.

CRediT authorship contribution statement

Tohid Adibi: Conceptualization, Writing – original draft. **Seyed Esmail Razavi:** Data curation, Methodology, Writing – review & editing. **Shams Forruque Ahmed:** Resources, Supervision, Writing – original draft, Writing – review & editing. **Hussein Hassanpour:** Project administration, Supervision, Writing – review & editing. **Neda Mohammadzadeh:** Supervision, Writing – review & editing. **S.M. Muyeen:** Supervision, Writing – review & editing.

Declaration of Competing Interest

The authors declare that they have no known competing financial interests or personal relationships that could have appeared to influence the work reported in this paper.

Data availability

No data was used for the research described in the article.

Acknowledgment

Open Access funding provided by the Qatar National Library.

References

[1] Shelley MJ, Zhang J. Flapping and bending bodies interacting with fluid flows. Annu Rev Fluid Mech 2011;43(1):449–65. https://doi.org/10.1146/annurev-fluid-121108-145456.
[2] Turek S, Hron J. "Proposal for Numerical Benchmarking of Fluid-Structure Interaction between an Elastic Object and Laminar Incompressible Flow," in *Fluid-Structure Interaction*, Berlin, Heidelberg, H.-J. Bungartz and M. Schäfer, Eds., 2006// 2006: Springer Berlin Heidelberg, pp. 371-385.
[3] Heil M, Hazel AL, Boyle J. Solvers for large-displacement fluid–structure interaction problems: segregated versus monolithic approaches. Comput Mech 2008;43(1):91–101. https://doi.org/10.1007/s00466-008-0270-6.
[4] Lee J, You D. Study of vortex-shedding-induced vibration of a flexible splitter plate behind a cylinder. Phys Fluids 2013;25(11):110811.
[5] Fu T, Chen Z, Yu D, Wang X, Lu W. Sound transmission from stiffened double laminated composite plates. Wave Motion 2017;72:331–41. https://doi.org/10.1016/j.wavemoti.2017.04.007.
[6] Fu T, Chen Z, Yu H, Zhu X, Zhao Y. Sound transmission loss behavior of sandwich panel with different truss cores under external mean airflow. Aerosp Sci Technol 2019;86:714–23. https://doi.org/10.1016/j.ast.2019.01.050.
[7] Zhao G, Fu T, "A unit compound structure design: poisson's ratio is autonomously adjustable from negative to positive," Mate*rials*, 16(5), 10.3390/ma16051808.
[8] Fang H, Bai S-L, Wong CP. Microstructure engineering of graphene towards highly thermal conductive composites. Compos A Appl Sci Manuf 2018;112:216–38. https://doi.org/10.1016/j.compositesa.2018.06.010.
[9] Tian F-B, Dai H, Luo H, Doyle JF, Rousseau B. Fluid–structure interaction involving large deformations: 3D simulations and applications to biological systems. J Comput Phys 2014;258:451–69. https://doi.org/10.1016/j.jcp.2013.10.047.
[10] De Nayer G, Kalmbach A, Breuer M, Sicklinger S, Wüchner R. Flow past a cylinder with a flexible splitter plate: a complementary experimental–numerical investigation and a new FSI test case (FSI-PfS-1a). Comput Fluids 2014;99:18–43.
[11] Khanafer K, Alamiri A, Pop I. Fluid–structure interaction analysis of flow and heat transfer characteristics around a flexible microcantilever in a fluidic cell. Int J Heat Mass Transf 2010;53(9–10):1646–53.
[12] Shi J, Hu J, Schafer SR, Chen C-L-C. Numerical study of heat transfer enhancement of channel via vortex-induced vibration. Appl Therm Eng 2014;70(1):838–45.
[13] Soti AK, Bhardwaj R, Sheridan J. Flow-induced deformation of a flexible thin structure as manifestation of heat transfer enhancement. Int J Heat Mass Transf 2015;84:1070–81. https://doi.org/10.1016/j.ijheatmasstransfer.2015.01.048.
[14] Yoshinaga T, Arai T, Inaam R, Yokoyama H, Iida A. A fully coupled fluid–structure–acoustic interaction simulation on reed-type artificial vocal fold. Appl Acoust 2021;184:108339. https://doi.org/10.1016/j.apacoust.2021.108339.
[15] Song X, Jin G, Ye T, Zhong S. A formulation for turbulent-flow-induced vibration of elastic plates with general boundary conditions. Int J Mech Sci 2021;205:106602. https://doi.org/10.1016/j.ijmecsci.2021.106602.
[16] Springer M, Scheit C, Becker S. One-Sided Fluid–Structure–Acoustic Interaction for Turbulent Flow over a Step. In: Grigoriadis DGE, Geurts BJ, Kuerten H, Fröhlich J, Armenio V, editors. Direct and Large-Eddy Simulation X, vol. 24. Cham: Springer International Publishing; 2018. p. 229–34.
[17] Prajapati S, Anantharamu S, Mahesh K, "Turbulent fluid-structure-acoustic interaction of an elastic plate in turbulent channel flow for different plate boundary conditions," January 01, 2021, 2021. [Online]. Available: https://ui.adsabs.harvard.edu/abs/2021APS..DFDE08009P.

[18] Pitchaimani J, Gupta P, Rajamohan V, Polit O, Manickam G. Acoustic fluid–structure study of 2D cavity with composite curved flexible walls using graphene platelets reinforcement by higher-order finite element approach (in en). Compos Struct 2021;272:114180. https://doi.org/10.1016/j.compstruct.2021.114180.
[19] Torregrosa A, Gil A, Quintero P, Ammirati A, Denayer H, Desmet W. Prediction of flow induced vibration of a flat plate located after a bluff wall mounted obstacle. J Wind Eng Ind Aerodyn 2019;190:23–39. https://doi.org/10.1016/j.jweia.2019.04.008.
[20] Lam GCY, Leung RCK, Fan HKH, Aurégan Y. Effect of back cavity configuration on performance of elastic panel acoustic liner with grazing flow. J Sound Vib 2021;492:115847. https://doi.org/10.1016/j.jsv.2020.115847.
[21] D'Elia ME, Humbert T, Aurégan Y. Linear investigation of sound-flow interaction along a corrugated plate. J Sound Vib 2022;534:117048. https://doi.org/10.1016/j.jsv.2022.117048.
[22] Borvornsareepirom N, Rojanaratanangkule W. A two-dimensional numerical investigation of aerodynamic noise from an inclined plate, (in en). Eng J 2022;26(6):41–52. https://doi.org/10.4186/ej.2022.26.6.41.
[23] Purohit A, Darpe AK, Singh S. Influence of flow velocity and flexural rigidity on the flow induced vibration and acoustic characteristics of a flexible plate, (in en). J Vib Control 2018;24(11):2284–300. https://doi.org/10.1177/1077546316685227.
[24] Banks JW, Henshaw WD, Schwendeman DW. An analysis of a new stable partitioned algorithm for FSI problems. Part I: incompressible flow and elastic solids. J Comput Phys 2014;269:108–37. https://doi.org/10.1016/j.jcp.2014.03.006.
[25] Griffith BE, Patankar NA. Immersed methods for fluid-structure interaction. Annu Rev Fluid Mech 2020;52(1):421–48. https://doi.org/10.1146/annurev-fluid-010719-060228.
[26] Mohammadi B, Pironneau O, "Analysis of the k-epsilon turbulence model," 1993.
[27] Kaltenbacher M, Escobar M, Becker S, Ali I. Numerical simulation of flow-induced noise using LES/SAS and Lighthill's acoustic analogy. Int J Numer Meth Fluids 2010;63(9):1103–22.
[28] Springer M, Scheit C, Becker S. Fluid-structure-acoustic coupling for a flat plate. Int J Heat Fluid Flow 2017;66:249–57.